AIChE

Particle Size Monitoring in Dense Suspension Using Ultrasound with an Improved Model Accounting for Low-Angle Scattering

A. Shukla, A. Prakash, and S. Rohani
Dept. of Chemical and Biochemical Engineering, University of Western Ontario, London, ON, Canada N6A 5B9

DOI 10.1002/aic.12182
Published online April 22, 2010 in Wiley Online Library (wileyonlinelibrary.com).

The inherent ability of ultrasonic wave to propagate in dense and opaque suspensions makes it a desirable method for online measurement of particle size distribution in industrial operations. The ability of ultrasonic attenuation spectroscopy to determine particle size distribution has been extended to dense suspensions of particles lying predominantly in the intermediate wave propagation regime at the measurement frequencies. This was achieved by accounting for the effect of detector size and shift in the frequency spectrum under dense conditions in the theoretical model and deconvolution algorithm, respectively. The proposed modifications enable the application of this technique in various industrial processes requiring in situ and real-time measurement of particle size distribution such as crystallization, mineral processing and food processing. © 2010 American Institute of Chemical Engineers *AIChE J,* 56: 2825–2837, 2010
Keywords: ultrasonic attenuation spectroscopy, particle size distribution, liquid–solid Suspensions, crystallization, mineral processing

Introduction

The transmission technique for measuring acoustic attenuation and velocity has evolved from the work of Pellam and Galt[1] and Pinkerton.[2] They used narrow band-width transducers in pulse-echo mode and variable path lengths to calculate the acoustic velocity and attenuation. Andrea and Joyce[3] modified this technique to incorporate through-transmission mode of operation and multiple frequency measurements using tone-burst signals. Multiple frequency measurements were further enhanced by the use of wide bandwidth video signals.[4] These signals consist of a range of frequencies as opposed to the finite cycle tone-bursts at different frequencies. The frequency component from wide bandwidth signals is extracted using Fast Fourier Transforms (FFT) and forms the basis of modern ultrasonic particle sizing technique.

Correspondence concerning this article should be addressed to A. Prakash at aprakas2@uwo.ca.

Recent advances in the hardware required for ultrasound generation and measurement has provided the ability to accurately measure the attenuation spectra over a wide range of frequencies. However, the accuracy of particle size distributions (PSD) generated is limited by the adequacy of the underlying theoretical model. In general, the model for acoustic particle sizing should meet the following criteria to enable its applicability in industrial processes:

1. Valid for large particle size range.
2. Valid for concentrated suspensions.

These criteria are achieved if the theoretical models account for the various attenuation mechanisms along with particle–particle interaction. The attenuation mechanism and extent of attenuation in an inhomogeneous medium is dependent on the physical properties of the liquid and solid phases along with particle size, pulse frequency and particles concentration. Various models available in literature for prediction of attenuation include the work of Riebel,[5] McClements,[6] Dukhin and Goetz,[7] Epstein and Carhart,[8] and Allegra and Hawley.[9] The different mechanisms of wave propagation have been discussed in detail by Dukhin and Goetz[7]

and can be broadly categorized under absorption (viscous and thermal losses) and scattering losses. The extent of these losses is a function of the wave propagation regimes, which are defined using the nondimensional wave number (kr). The wave number is the ratio of particle radius to pulse wavelength and can be calculated using Eq. 1. Different wave propagation regimes identified based on this number is also shown in the equation given below.

$$kr = \frac{\omega}{c} r = \frac{2\pi f}{c} r = \frac{2\pi r}{\lambda}$$

$$\begin{aligned} &kr << 1; \quad \lambda >> r && \text{Long wave regime} \\ &kr \sim 1; \quad \lambda \sim r && \text{Intermediate wave regime} \\ &kr >> 1; \quad \lambda << r && \text{Short wave regime} \end{aligned} \tag{1}$$

There are two approaches to determine the total attenuation caused by various energy loss mechanisms. The traditional approach has been to develop a unified theory accounting for each of the loss mechanisms. The most widely used unified theory is the ECAH[8,9] model and accounts for the viscous, thermal and scattering losses. It is based on the superposition of single particle attenuation to obtain the total energy loss. This theory is limited to long wave regime of propagation, wherein the particles are much smaller than the wavelength. It also does not account for particle–particle interactions and hence is limited to dilute concentrations. The various modifications/extensions to increase the applicability of the ECAH theory include the work of McClements et al.,[10] Watermann and Truell,[11] Lloyd and Berry,[12] Harker and Temple,[13] Gibson and Toksoz[14] and Temkin.[15] However, these modifications are still unable to meet the two basic criteria required for a truly universal particle sizing technique. An alternative approach to determine total attenuation was suggested by Dukhin and Goetz.[7] This approach is based on the well known extinction theory proposed by Bohren and Huffman.[16] This theory was originally proposed for light but is also relevant for sound and states that the various energy losses are additive (Extinction = Absorption + Scattering). Hence, the various attenuation losses can be independently determined using individual theories for scattering (α_{sc}), viscous (α_v) and thermal (α_t), loss mechanisms.

$$\alpha = \alpha_{sc} + \alpha_v + \alpha_t \tag{2}$$

However, Dukhin and Goetz[7] have concentrated their efforts to develop a rigorous model for viscous and thermal dissipation and only refer to simplified scattering model as their focus was on particle sizing in the colloidal and emulsion region (long wave regime). This study analyzes experimentally measured attenuation in the intermediate wave regime (kr) where both viscous and scattering losses are present. In this regime the viscous losses are dominant at lower wave numbers and scattering losses gain significance at higher wave numbers. However, neither of these losses is small enough to be completely neglected. The theoretical model used in this study is adapted from the work of Morse and Ingard[17] and extended to account for multiple frequencies and polydispersity.

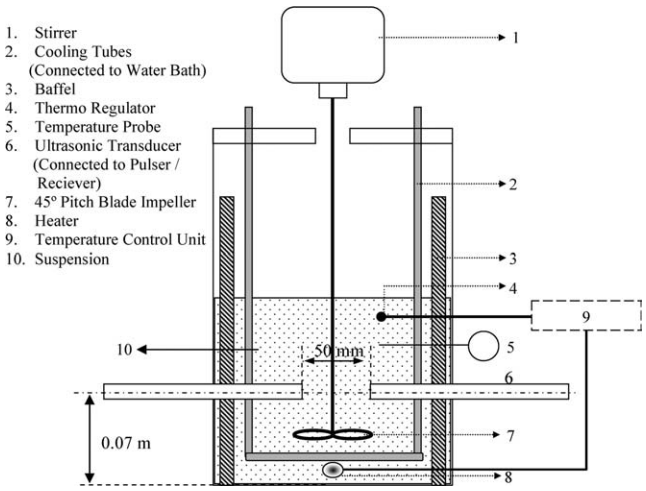

Figure 1. Schematic diagram of the stirred tank.

Experimental Details

Attenuation measurements were made at different frequencies in liquid-solid suspension of glass beads in deionized (DI) water using Fallon Ultrasonic® pulser/receiver unit. The experiments were conducted in a stirred tank made of plexiglas with diameter 0.1 m and height 0.252 m. A schematic representation of the stirred tank used is shown in Figure 1. It is equipped with radial ports for mounting the transducers and a vertical stirrer for suspending the particles. The stirrer speed was maintained about 10% above the minimum speed required for good particle suspension.[18] The glass beads had a mean size of 43, 85, 114, 119, 156, 202-μm and the suspension concentration was varied from 2 to 20 vol % with 2 vol % increments. Measurements were also made in concentrated slurries of 119-μm glass beads in canola oil and 112-μm aluminum oxide in DI-water. Acoustic parameters were measured using the Fallon pulser/receiver unit in through transmission mode. The acoustic pulse was generated using broadband transducers and the instrument reported the peak amplitude of the pulse. The pulser/receiver unit activates the receiving transducer at a time fixed by the delay and for duration of the gate width to measure the flight time of the signal. The pulse repetition rate was 1 kHz and the sampling interval was 1 s. Hence, each sampled value of transit time and amplitude represent the average of 1000 acoustic pulses. Transducer separation used during this study was 50 mm and experiments were conducted using two sets of transducers with central frequencies of 3.4 and 1.2 MHz. This arrangement of transducers is intrusive in nature but was preferred to maximize signal strength. The transducers were enclosed in a cylindrical housing to minimize resistance to the flow of slurry. Small ratio of the particle size to the distance between transducers also reduced distortions to particles motion in the stirred tank. A TDS 210 (Tektronix) digital oscilloscope was used to visualize, select, and capture the pulse.

Results and Discussions

Figure 2 shows the change in attenuation at peak frequency with concentration for 43 and 114-μm particles using 3.4 and 1.2 MHz transducers. Attenuation was calculated

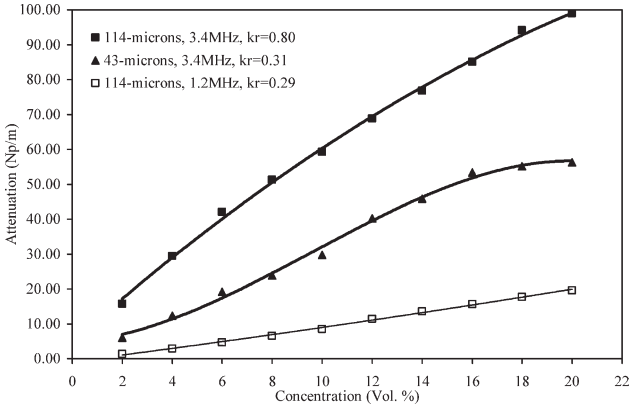

Figure 2. Change in attenuation (Np m^{-1}) with concentration for 114- and 43-μm particles using 1.2 and 3.4 MHz transducers.

using Eq. 3 and shows an increase with concentration for both particle sizes.

$$\alpha_M(\text{Np m})^1 = \sum_{i=1}^{m} \frac{1}{x} \ln\left(\frac{A_{i-1}}{A_i}\right) \tag{3}$$

In the above equation, A_{i-1} and A_i are the measured amplitudes before and after incremental solids addition respectively. The total attenuation at a given solids concentration is the summation of incremental attenuations at the preceding concentrations. This procedure was developed to account for increase in gain which was increased at regular concentration intervals required to make up for the loss in signal strength due to attenuation. At a given concentration the maximum gain level is limited to avoid saturation of the signal.

Figure 2 shows that the measured attenuation is higher for larger particles at 3.4 MHz frequency and is similar to results obtained in literature studies.[19–21] The wave numbers (kr) for the mean particle size at different central frequencies are also shown in Figure 2. Experimental measurements

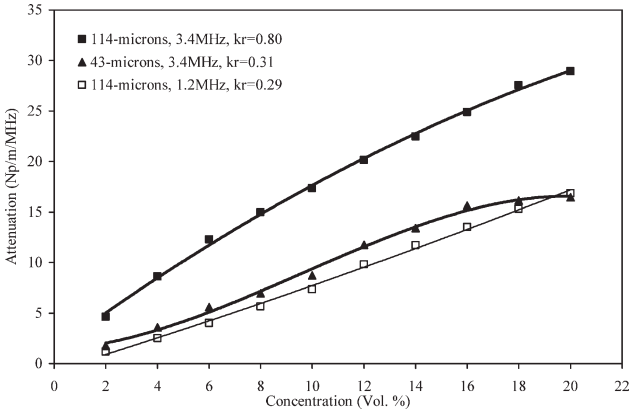

Figure 3. Change in attenuation/central frequency (Np m^{-1} MHz^{-1}) with concentration for 114- and 43-μm particles using 1.2 and 3.4 MHz transducers.

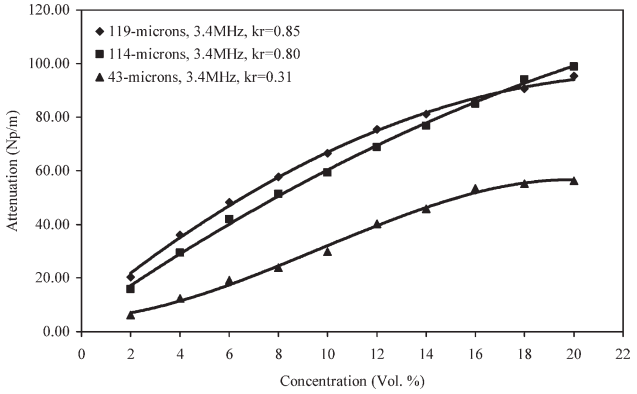

Figure 4. Comparison of change in attenuation (Np m^{-1}) with concentration for 43-, 114-, and 119-μm particles using 3.4 MHz transducer.

show a significant difference in measured attenuation for similar kr values obtained using different particle sizes and frequencies. The kr values of 114- and 43-μm particles at 1.2 and 3.4 MHz frequency are 0.29 and 0.31, respectively. Similar attenuation was expected for these suspensions as the relative difference between their kr values is small and indicates the presence of a common wave propagation regime. Theoretical models suggested in literature show that the attenuation within a propagation regime are scaled according to the frequency.[20,21] Hence, the effect of measurement frequency on attenuation needs to be normalized for the comparison of these coefficients obtained at different frequencies. This can be achieved by calculating the attenuation per unit frequency as shown in Eq. 4.[7]

$$\alpha_M(\text{Np m}^{-1}\ \text{MHz})^{-1} = \frac{1}{f}\sum_{i=1}^{m} \frac{1}{x} \ln\left(\frac{A_{i-1}}{A_i}\right) \tag{4}$$

Figure 3 shows that attenuation per MHz of frequency for 43- and 114-μm particles are similar for similar kr values when they are scaled with respect to the frequency.

Figure 4 shows that change in attenuation in Np m^{-1} is linear with increase in concentration up to 6 vol % for 119-,

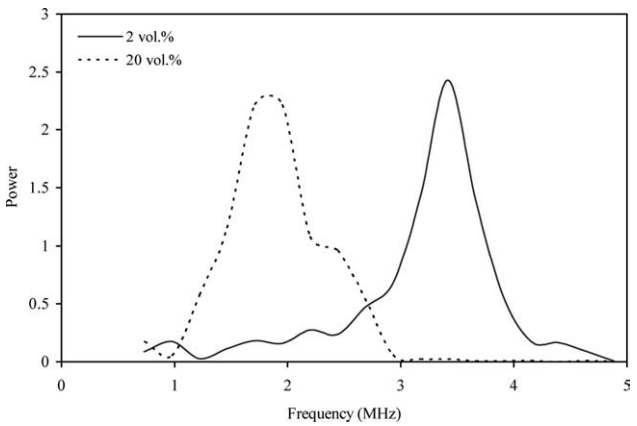

Figure 5. Power spectrum 119-μm particles using 3.4 MHz transducer.

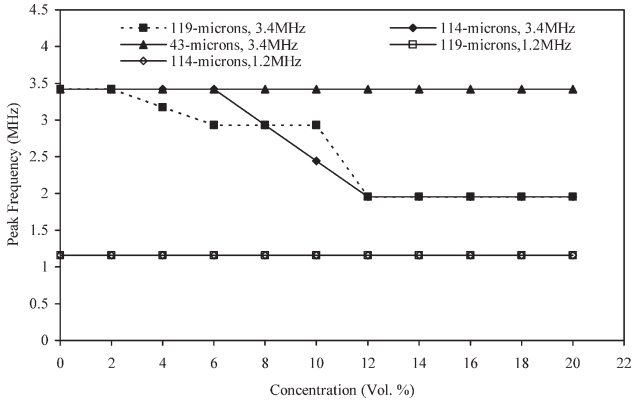

Figure 6. Change in peak frequency with concentration for 43-, 114-, and 119-μm particles using 3.4 and 1.2 MHz frequency transducers.

114-μm particles and up to 18 vol % for 43-μm particles. Nonlinearity of attenuation with increase in concentration can be attributed to particle–particle interactions at high concentration and is dependent on the dominant mechanism of attenuation.[7] It is shown by these authors that viscous attenuation is linear up to 14 vol % concentrations and scattering attenuation is linear up to 40 vol % concentrations. This indicates that the observed nonlinearity of the attenuation with concentration for 114 and 119-μm particles cannot be due to particle–particle interactions. An alternative explanation for this observation can be attributed to the pulse bandwidth. Figure 5 shows the acoustic pulse in the frequency domain at 2 and 20 vol % for 119-μm particle suspension. Both the measured pulses are characterized by a peak frequency at which maximum attenuation occurs. However, the peak frequency location changes significantly with increase in concentration.

In the intermediate wave propagation regime, scattering attenuation increases with increase in the frequency of the acoustic pulse.[20,7] Hence, for a broadband acoustic pulse,

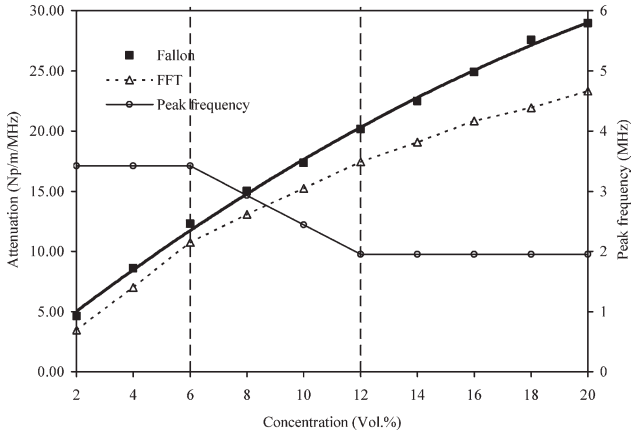

Figure 7. Comparison of attenuation/peak frequency (114 μm at 3.4 MHz) calculated using measurements from the Fallon instrument and FFT along with the change in measured peak frequency.

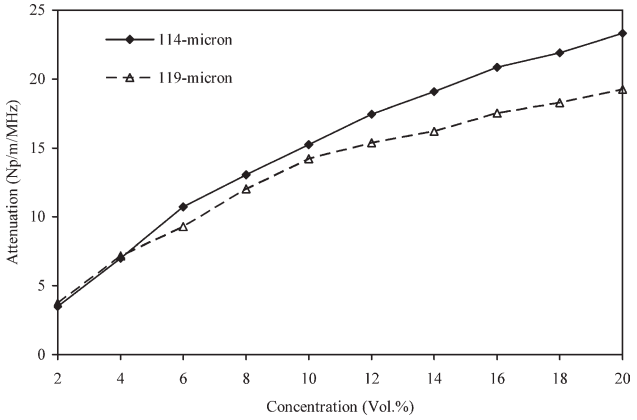

Figure 8. Comparison of attenuation/peak frequency (FFT) for 114- and 119-μm particles using 3.4 MHz transducer.

energy at higher frequencies will dissipate at a faster rate as compared to lower frequencies and will eventually lead to total loss of power at higher frequencies. As a result of this the measured peak amplitude by the unit gradually shifts to lower frequencies. As energy dissipation at lower frequencies is smaller, the attenuation appears to become less sensitive to concentration increase in dense suspensions. Furthermore, the change in peak frequency occurs after incremental solids addition. Hence, the peak amplitudes "A_i" and "A_{i-1}" measured by the pulser/receiver unit are at different frequencies. This error can be avoided by using the FFT to obtain the attenuation measurements at the peak frequency of the received pulse (Eq. 5).

$$\alpha_{f_{\text{peak}}}(\text{Np m}^{-1}\ \text{MHz})^{-1} = \frac{1}{f_{\text{peak}}}\sum_{i=1}^{m}\frac{1}{2x}\ln\left(\frac{P_{i-1}}{P_i}\right) \qquad (5)$$

The peak frequencies of the received pulse for different particle sizes obtained using FFT are shown in Figure 6. The figure shows that the shift in peak frequency only occurs for particles predominantly in the intermediate wave regime (average $kr \sim 0.8$) where the scattering mechanism is dominant.

Figure 7 shows a comparison of the normalized attenuation at the peak frequency obtained using the pulser/receiver and FFT along with the peak frequency at different concentrations of 114-μm particles (3.4 MHz transducer). The calculated attenuations using the two techniques are similar till a change in the peak frequency after 6 vol % occurs. Above this concentration higher attenuations are calculated from the amplitude measurements obtained using the Fallon instrument as measured amplitudes "A_i" and "A_{i-1}" are at different frequencies. The attenuation measurements obtained from the FFT is linear even at high concentrations provided the measurement frequency does not change.

An interesting observation was made from comparison of normalized attenuation at peak frequency obtained from FFT with 114 and 119-μm particles and 3.4 MHz transducers (Figure 8). Significant difference between measured attenuation for these particles with similar mean size was observed above 4 vol % concentration. At intermediate concentrations (4–12 vol %) the observed deviation could be attributed to

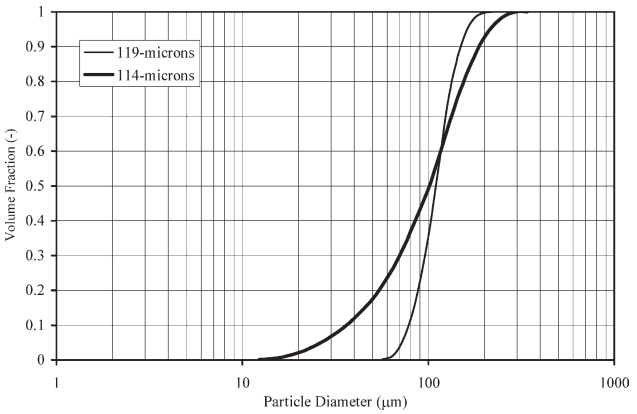

Figure 9. Particle size distribution of 114- and 119-μm particles (Malvern Mastersizer®).

change in the peak frequency. However, the average change in peak frequency for both particles from 2 to 20 vol % was similar and hence the measured attenuations at 20 vol % should have been comparable. The observed difference in the attenuation measurements in Figure 8 can be attributed to the nature of size distribution of the two particle samples. Figure 9 shows the PSD obtained using the Malvern Mastersizer® of 114 and 119-μm particles. The size distribution of 114-μm particles is wide and ~25% of particles are smaller and ~10% of particles are larger than the minimum and maximum particle size in the 119-μm particle sample. The average *kr* values of the smaller and larger particle fractions in 114-μm samples at 3.4 MHz are 0.21 and 1.8, respectively. As the *kr* values of larger particle fraction in 114-μm sample is ~2 times the average *kr* value of 119-μm particles, the extent of scattering will be higher. The resolution of attenuation measurements increases for concentrations greater than 1 vol % and has been experimentally shown for mixed particle systems of varying sizes.[19,22] Above 14 vol % the fraction of particles between 200 and 300μm in the 114-μm sample exceeds 1 vol %. Furthermore, although scattering attenuation for the lower size fraction in the 114-μm particle decreases, the viscous dissipation effect will rise. Hence, difference in attenuation measurements of 114- and 119-μm particles appears to be due to the nature of their size distributions.

The trend of attenuation of 114- and 119-μm particles with concentration showed significant difference when, the *kr* values were reduced from 0.8 to 0.3. In this region, viscous attenuation is the dominant mode of energy loss and no change in the peak frequency was observed. Figure 10 shows the attenuation measurements at $kr \sim 0.3$ for 114 and 119-μm particle samples (at 1.2MHz) along with 43-μm particles (at 3.4 MHz frequency). Unlike measurements at 3.4 MHz, the attenuation of 114-μm particles are higher than 119-μm particles even at low concentration. Higher attenuation measured in the suspension of 43-μm particles shows that the contribution of viscous attenuation increases with decrease in particle size and is in agreement with literature.[7] Hence, the difference in attenuation of 114- and 119-μm particles can be attributed to small particles in the 114-μm sample. Figure 9 shows that 25% of 114-μm particles are below 60-μm. With increase in concentration from 4 to 20 vol % the concentration of smaller particles (<60 μm, $kr \sim 0.15$) in 114-μm particle suspension increases from 1 to 5 vol % and starts contributing significantly to the total attenuation. This results in an increase in attenuation measurements of 114 compared to 119-μm particles at higher concentrations.

Unlike 43-μm particles at 3.4 MHz ($kr \sim 0.3$) no effect of particle–particle interactions was observed with 114- and 119-μm particles even though the *kr* values are similar. Particle–particle interactions during viscous dissipation are dependent on the viscous layer thickness and the inter-particle separation. The viscous layer thickness is affected by the viscosity, density of the medium and the frequency of the acoustic pulse.[17]

$$\delta_v = \sqrt{\frac{2\mu_f}{\omega\rho_f}} \tag{6}$$

Particle–particle effects are caused when the viscous layers of adjacent particles interact and the likelihood of such interactions increases with increase in the number of particles. The viscous layer thickness obtained at 1.2 MHz frequency is ~1.6 times the thickness at 3.4 MHz frequency. However, the average number of particles at 18 vol % for 43-μm particle size is more than that of 114-,119-μm by ~19 times. Hence, the onset of particle–particle interactions for 43-μm particles occurs at a lower concentration as compared to 114- and 119-μm particles.

Attenuation predictions in polydispersed suspensions

Theoretical models for the calculation of energy loss due to different propagation mechanisms have to account for the effect of pulse frequency, particle size and the physical properties of the different phases. Models available in literature for determination of absorption and scattering losses are based on the superposition principle. These models are developed for monosized particles at a single frequency and the total attenuation is obtained by multiplying the attenuation caused by a single particle with the total number of particles present.

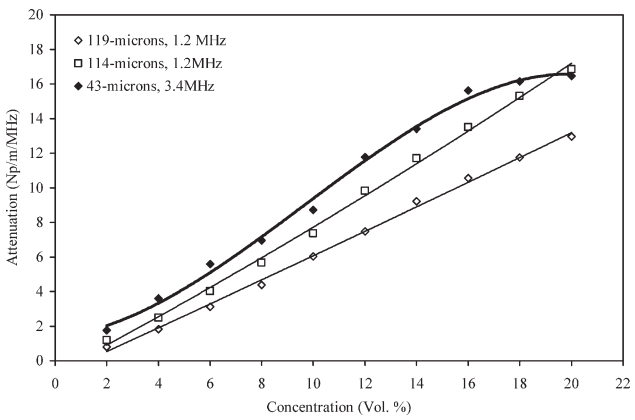

Figure 10. Comparison of attenuation/peak frequency for 114- and 119-μm particles using 1.2 MHz transducer.

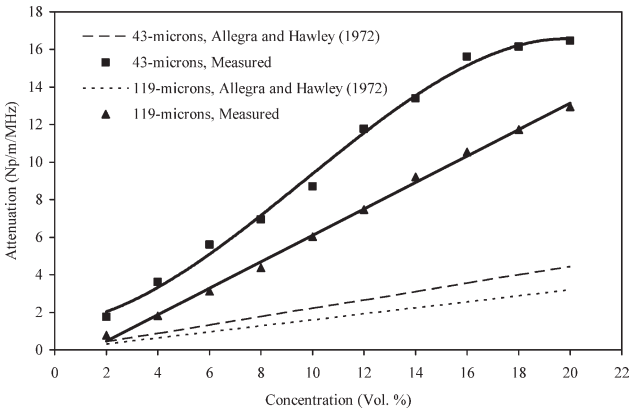

Figure 11. Comparison between measured and predicted (Allegra and Hawley)[9] attenuation/ peak frequency at 0.3 *kr*.

$$\alpha_{T,MD} = N\alpha \tag{7}$$

For polydispersed suspensions the normalized total attenuation can be calculated by superposing the effect of different size fractions.

$$\alpha_{T,PD} = \frac{1}{f}\sum_{i=1}^{i=n} N_i\alpha_i\,; \quad N_i = \frac{3\phi}{4\pi r_i^3} \tag{8}$$

However, Eq. 8 can only be used if there are no particle–particle effects in the system. This condition exists if the concentration of fines (viscous dissipation) is below the limit of interparticle interactions and the regime of propagation for larger particles is in the region of single scattering.

Necessity for Measurements in Intermediate Regime. Particle sizing using attenuation spectroscopy relies on the extent of attenuation variation with frequency. Hence, attenuation has to be measured over a broad range of frequencies to enable PSD determination. Traditional model based methods for PSD determination has been restricted to the long wave propagation regime. However, this regime cannot be achieved for particles much larger than 10 μm over a sufficiently broad frequency range. This limitation is further discussed below by comparing the measured attenuations at low *kr* values with calculated attenuations using Allegra and Hawley[9] model.

Allegra and Hawley[9] model is based on the equation of continuity (mass conservation) and Navier-Stokes equation (momentum conservation) which are used to derive the wave equations for the compressional, shear and thermal propagation. The model generates attenuation for mono-sized particles in the long wave propagation regime, i.e., λ [dmt] r. The attenuation in polydispersed suspensions can be calculated using Eq. 8 and is compared with measurements of 119 μm at 1.2 MHz and 43 μm at 3.4 MHz (Figure 11). The explicit equations used for the calculation of attenuation of monosized particles were obtained from Allegra and Hawley.[9] The measured and calculated attenuations show an agreement only up to 2 vol % concentration. The Allegra and Hawley[9] model fails when the wavenumber exceeds 0.1. The deviation of measurements from calculated attenuations can be attributed to the relatively high wave number of the particles used in this study. This indicates that even for 100-μm particles the maximum measurement frequency should be below 1 MHz to enable PSD predictions using long wave regime models. With further increase in particle size the available bandwidth is further diminished as frequencies below 40 kHz lie in the region of cavitation and cannot be used for particle sizing. This drawback can be overcome by making measurements in the intermediate regime of propagation. In this regime, absorption losses are dominant at lower wave numbers and scattering losses gain significance at higher wave numbers. However, neither of these losses is small enough to be completely neglected. Hence, the maximum frequency should be limited to avoid the regions of multiple scattering for large particle fractions. The minimum frequency should be high enough to avoid particle–particle interactions in the absorption region which occur due to the overlap of the viscous layers of neighboring particles. Limiting the wave propagation to this regime is advantageous as simple scattering and absorption models can be used for attenuation calculations.

Attenuation model in the intermediate regime

Morse and Ingard[17] present a model to estimate attenuation in the intermediate regime of wave propagation. This model calculates the power lost in terms of scattering and absorption cross sectional areas of monodispersed particles at a given frequency. The power lost due to absorption or scattering divided by the power per unit area of the incident wave gives the absorption and scattering cross sections ($\sum_a$, $\sum_s$) of the particle. Hence, attenuation is the power contained in this cross sectional area of the incident beam which is lost during wave propagation. The power of a wave propagating through a medium filled with "N" particles per unit volume of medium is given by Eq. 9 and the attenuation can be calculated using Eq. 10.

$$P_1 = P_o e^{-N\left(\sum_s + \sum_a\right)x} \tag{9}$$

$$\alpha = \frac{1}{2x}\ln\left(\frac{P_{i-1}}{P_i}\right) = \frac{1}{2}N\left(\sum_s + \sum_a\right) \quad \left(\frac{Np}{\text{length}}\right) \tag{10}$$

where, $N = \frac{3\phi}{4\pi r^3}$

The scattering and absorption cross-sections for a spherical particle suspended in a fluid can be calculated by Eqs. 11 and 12 given by Morse and Ingard.[17]

$$\sum_s = 2\pi\int_0^\pi |\Phi(\vartheta)|^2 \sin\ \vartheta\, d\vartheta \quad (\text{length}^2) \tag{11}$$

$$|\Phi(\vartheta)|^2 = \left|\frac{i}{2k}\sum_{m=0}^{\infty} 2(2m+1)\,\frac{j'_m(kr) + i\beta_m j_m(kr)}{h'_m(kr) + i\beta_m h_m(kr)}\dot{P}_m(\cos\ \vartheta)\right|^2 \tag{12}$$

$$\sum_a = \frac{k^4 r^4}{4\pi r^2}\sum_{m=0}^{\infty}\frac{(2m+1)\mathrm{Re}(\beta_m)}{\left[h'_m(kr) + i\mathrm{Im}(\beta_m)h_m(kr)\right]^2} \quad (\text{length}^2) \tag{13}$$

where, "$h_m(kr)$" and "$j_m(kr)$" are spherical Hankel and Bessel functions of the order "m" and "$h'_m(kr)$" and "$j'_m(kr)$" are their respective derivatives.

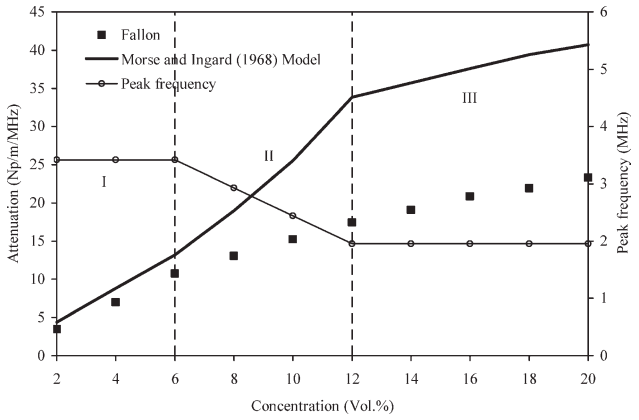

Figure 12. Comparison between measured and calculated[17] attenuation/peak frequency for 114-μm particles using 3.4 MHz transducer.

$$h_m(kr) = \frac{i^{-m}}{ikr}\sum_{s=0}^{m}\frac{(m+s)!}{s!(m+s)!}\left(\frac{i}{2kr}\right)^s e^{ikr} \tag{14}$$

$$j_m(kr) = \mathrm{Re}[h_m(kr)] \tag{15}$$

$$\beta_m(kr) = i\frac{\rho_f c_f}{\rho_p c_p}\left(\frac{j'_m(k_f r)}{j_m(k_p r)}\right) + \frac{1}{2}(1-i)\left(\frac{m(m+1)}{r^2}k\delta_v\right) \tag{16}$$

$$c_f = \frac{1}{\rho_f \kappa_f} \quad ; \quad c_p = \frac{1}{\rho_p \kappa_p} \tag{17}$$

The sound speed "c" in fluid and particle are given by Eq. 17 where, "κ" and "ρ" are their compressibility and density.

Peak Frequency. Figures 12 and 13 show the comparison of normalized measured and calculated attenuation (Morse and Ingard[17]) at the peak frequency for 114- and 119-μm particles, respectively. The changes in peak frequency with concentration are also shown in the figures. The particle size distribution used for calculating total attenuation was measured using Malvern® Mastersizer. Figure 12 shows a good agreement between measured and calculated attenuations for 114 μm particle suspension up to 6 vol % concentration (Region I). The calculated attenuation in Region II deviates away from the measurements even though there is a decrease in the peak frequency. This observation is contrary to expectations since attenuation in this regime has an inverse relationship with frequency. In Region III, the rate of change in attenuation with frequency was constant and is likely due to no change in the peak frequency. Figure 13 shows the measured and calculated attenuation with change in concentration at the measured peak frequencies for 119-μm particles with 3.2 MHz transducer. Good agreement between measured and calculated attenuations was only obtained at 2 vol %. Similar to 114-μm particles the rate of change in attenuation remains constant in Region II and IV when the peak frequency does not shift and rises rapidly in Region III with a decrease in the peak frequency.

The ability of the model to make reasonable attenuation predictions at low concentrations indicates that the deviations at higher concentrations are due to increase in particles concentrations. Dukhin and Goetz[7] have shown that particle–particle interaction in the scattering regime is minimal up to 40 vol % concentration and should not be the reason for erroneous model calculations. A comparison of the magnitude of calculated attenuations from 12 to 20 vol % in Figures 12 and 13 shows that higher attenuations were obtained for 119-μm particles even though the measurement frequency remains constant at about 2 MHz. This is contrary to the measurements as the attenuation of 114-μm particle is higher than 119-μm particles at these concentrations (Figure 8). The PSD of these particles (Figure 9) show that the 119-μm sample has a narrow distribution of predominantly large particles. This indicates that large attenuations calculated for 119-μm as compared to 114-μm particles is most likely due to the inability of the model to account for higher concentrations of larger particles. The Morse and Ingard[17] model has been analyzed in further details to understand the reason for higher attenuation predictions in dense suspensions.

Low-Angle Scattering

The power of the scattered wave at different angles in the scattering cross section can be calculated using Eq. 12 where "$|\Phi(\vartheta)|^2$" is the angle-distribution factor of the scattered wave and "ϑ" is the scattering angle.[17] Figure 14 shows the polar plots of "$|\Phi(\vartheta)|^2$" at 0.5, 1, 1.5, and 2 kr calculated at a frequency of 3.4 MHz. The scattering angle "ϑ" is shown on the angular co-ordinate and the scattered power is shown on the radial co-ordinate and the direction of wave propagation is indicated on the figure. If the detector is infinitesimally small and is located at the point where the angle "$\vartheta = 0$" then the integral in Eq. 11 will give the total power abstracted from the incident beam due to scattering. Generally, the detector has a finite size and will subtend a measurement angle "Δ" on the particles and is shown in Figure 14c. Morse and Ingard[17] have shown that "$\Delta \sim 0$" when the following relationship is satisfied.

$$\lambda << \frac{4r}{\Delta} \tag{18}$$

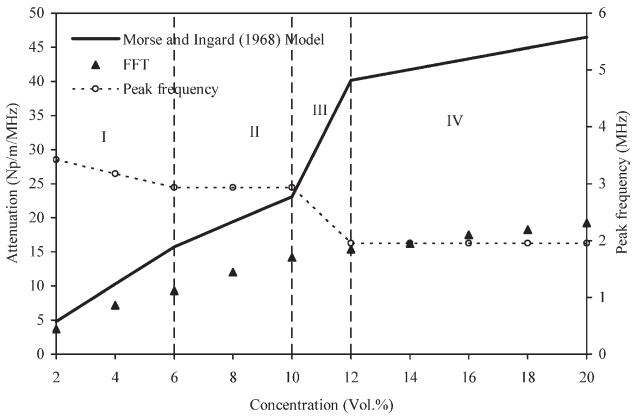

Figure 13. Comparison between measured and calculated[17] attenuation/peak frequency for 119-μm particles using 3.4 MHz transducer.

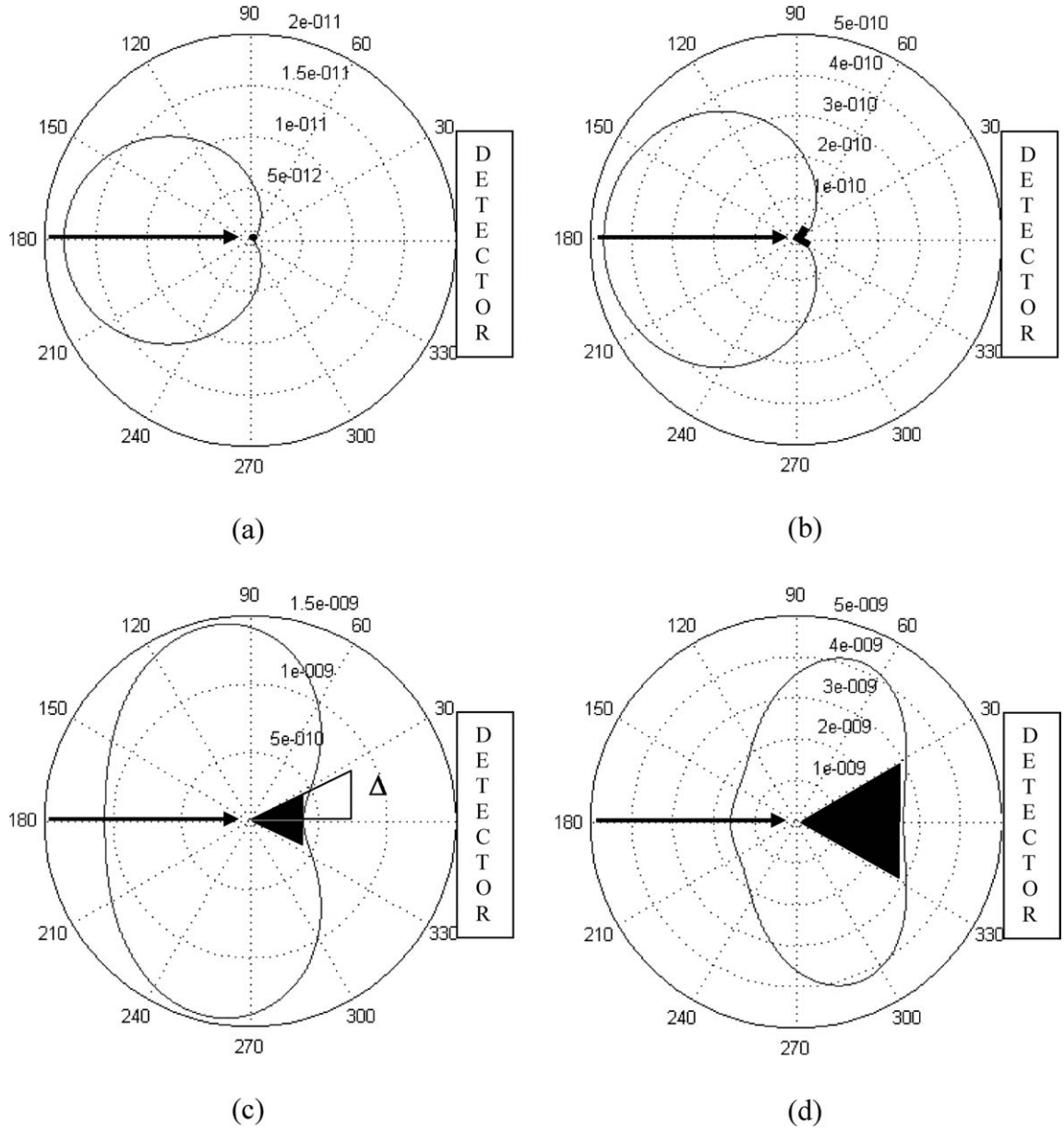

Figure 14. Polar plot of scattering intensity distribution for *kr* of 0.5 (a), 1 (b), 1.5 (c), and 2 (d).

Equation 11 can be simplified to the following form when the above condition is satisfied using the orthogonal property of the Legendre polynomial between the limits of 0 to π.[17]

$$\sum_s = \frac{4\pi}{k^2}\sum_{m=0}^{\infty}(2m+1)\left|\frac{j'_m(kr)+i\beta_m j_m(kr)}{h'_m(kr)+i\beta_m h_m(kr)}\right|^2 \quad (\text{length}^2) \tag{19}$$

Morse and Ingard[17] have shown that the relationship in Eq. 18 is true in the long wave regime of wave propagation where the forward scattering is negligible. However, in this study the average *kr* value of 114 and 119-μm particles is well above the long wave regime of wave propagation. At these *kr* values the measurement angle 'Δ' cannot be considered close to zero. The power scattered within this angle will be measured by the detector and the experimental attenuation will be lower than the attenuation calculated using Eq. 11. The effect of low angle scattering on measured attenuation will also increase with concentration as the number of particles increases. Good agreement of calculated attenuation with measurements up to 2 vol % in Figures 12 and 13 indicates that this is negligible at low concentrations. At higher concentrations the scattering cross section should be calculated by integrating between the limits of "$\vartheta = \Delta$" and "$\vartheta = \pi - \Delta$" to account for the measurement of low-angle scattered waves.[23,24]

$$\sum_s = 2\pi\int_{\Delta}^{\pi-\Delta}|\Phi(\vartheta)|^2\sin(\vartheta)d\vartheta \tag{20}$$

The measurement angle "Δ" is required for the calculation of the attenuation cross section using Eq. 20. It is

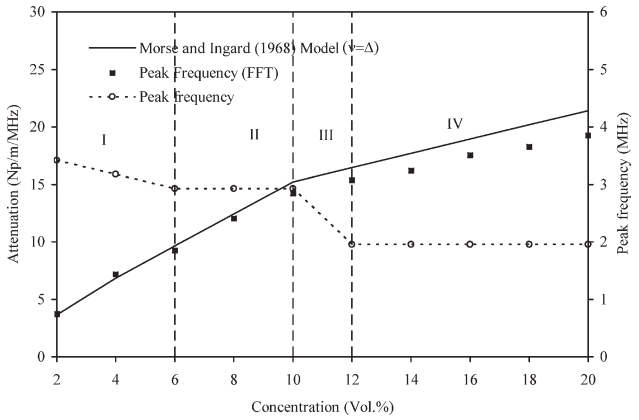

Figure 15. Comparison between measured and calculated attenuation/peak frequency (with low-angle scattering) for 119-μm particles using 3.2 MHz transducer.

proposed in this study that the angle "Δ" can be considered to be the average angle subtended by a point lying on the circumference of the receiver to the maximum and minimum location on the receiver/detector axis. However, this will only be valid as long as the effect of rescattering of the scattered wave is not prominent which is expected to be valid up to 40 vol % concentration.[7] Hence, the total attenuation in a polydispersed suspension at the peak frequency can now be calculated by combining Eqs. 8, 10, 13, and 20 as shown below.

$$\alpha_{\mathrm{T,PD}} = \frac{1}{2f}\sum_{i=1}^{i=n} N_i\left(\sum_{si} + \sum_{ai}\right) \quad \left(\frac{\mathrm{Np}}{\mathrm{length.MHz}}\right) \tag{21}$$

The approximation proposed above was tested to predict the attenuation at different concentrations for 119-μm particles and is shown in Figure 15. The figure shows good agreement between the measured and calculated attenuations when the low-angle scattering is included in model calculations. Similar improvement in model predicted attenuations were also obtained for 114-μm particles.

Attenuation Spectrum. Equation 22 can be used to obtain the normalized attenuation at different frequencies from the FFT of a broad band acoustic pulse.

$$\alpha_{\mathrm{f}} = \frac{1}{2xf}\ln\left(\frac{P_{i-1,\mathrm{f}}}{P_{i,\mathrm{f}}}\right) \quad \left(\frac{\mathrm{Np}}{\mathrm{length.MHz}}\right) \tag{22}$$

The calculated attenuation using the proposed modification of the Morse and Ingard[17] model can be tested at different frequencies using the above equation. However, due to the shift in the frequency spectrum a consistent set of frequencies is not available for the entire concentration range. The effect of shift in the frequency spectrum can be accounted for by using a weighting factor.

$$\alpha_{\mathrm{f},m}(\mathrm{Np\ m^{-1}\ MHz})^{-1} = w_{\mathrm{f}}\frac{1}{2x.f}\ln\left(\frac{P_{\mathrm{f},i-1}}{P_{\mathrm{f},i}}\right) \tag{23}$$

$$w_{\mathrm{f}} = \frac{P_{\mathrm{f},i}}{\sum_{f_{\min}}^{f_{\max}} P_{\mathrm{f},i}} \tag{24}$$

The weighting factor (w_{f}) scales the attenuation at each frequency according to its strength in the measured signal. This scaling will exclude attenuations at higher frequencies when their power content becomes less than the acceptable minimum limit. It also allows the inclusion of attenuations at lower frequencies which become significant with increase in concentration. Another advantage of attenuation scaling is that it gives greater weight to frequencies with higher power content. Hence, errors caused due to measurement uncertainties at frequencies with low power content are reduced. The total effective measured attenuation of the acoustic pulse can then be obtained using Eq. 25.

$$\alpha_{\mathrm{T,M}}(\mathrm{Np\ m^{-1}\ MHz})^{-1} = \sum_{f_{\min}}^{f_{\max}} w_{\mathrm{f}}\frac{1}{2x.f}\ln\left(\frac{P_{\mathrm{f},i-1}}{P_{\mathrm{f},i}}\right) \tag{25}$$

For comparison between measured and predicted attenuation the weighting factor should also be used in Eq. 21 to replicate the frequency spectrum in model calculations. Figure 16 compares the measured and calculated effective attenuations (at $\vartheta = 0$ and $\vartheta = \Delta$) for 119-μm particles using 3.4 and 1.2 MHz central frequency transducers. As expected the effect of measurement angle "Δ" is significant for higher frequency transducer due to dominance of scattering attenuation. However, at 1.2 MHz its effect can be neglected as both equations predict similar attenuations. Figure 17 shows good agreement between measured and predicted total attenuation for the 114-μm sample measured using 3.4 MHz central frequency transducers. The proposed modifications to the model along with the use of weighting factor to replicate the measurement conditions in model calculations shows that good agreement with measured attenuations can be obtained in dense suspensions. Hence, the modified form of the Morse and Ingard[17] model is a suitable

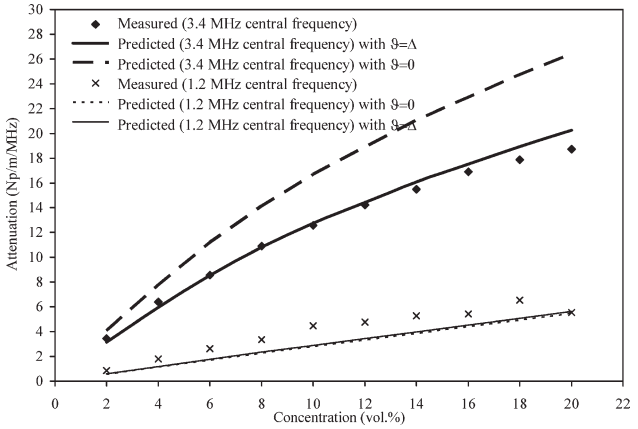

Figure 16. Change in measured and calculated total attenuation with concentration for 119-μm particles using original Morse and Ingard[17] model and with model modification proposed in this study.

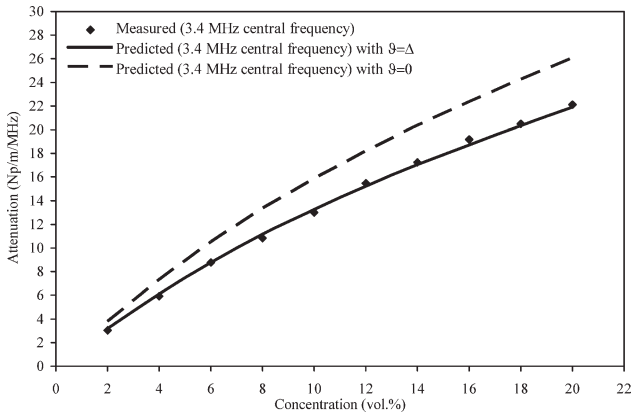

Figure 17. Change in measured and calculated total attenuation with concentration for 114-μm particles using original Morse and Ingard[17] model and with model modification proposed in this study.

candidate for the deconvolution algorithm to obtain model based PSD in dense suspensions.

Deconvolution

Model based particle size distribution is obtained by optimizing the parameters of an assumed size distribution to minimize the error between measured and predicted attenuation spectrums. Weight factors in the deconvolution algorithm can be used to replicate measurement conditions in model predictions as shown in Figure 18. Log-normal is a widely used analytical size distribution for describing distribution of particles. Particle size distribution can be estimated by obtaining the best fit of the parameters of log-normal size distribution function. The global search technique was used to find the optimum log-normal distribution parameters for best-fit particle size distribution. The theoretical attenuation spectra were calculated for all physically feasible log-normal parameters to obtain the error matrix.

$$\varphi_d^{\mu,\sigma} = \frac{1}{d\sigma\sqrt{2\pi}} e^{\frac{-(\ln(d)-\mu)^2}{2\sigma^2}} \tag{26}$$

The two parameters used for defining this distribution are its geometric mean (μ) and standard deviation (σ). The possible values which can be achieved by the parameters "μ" and "σ" can be restricted by defining the minimum ($d_{\min}$) and maximum ($d_{\max}$) particle size which can be present in the system. Hence, for a given "μ" ($d_{\min} < e^{\mu} < d_{\max}$) the values of "$\sigma$" should satisfy Eq. 27.

$$\varphi_{d_i}^{\mu,\sigma} \begin{cases} \varphi_{d_i}^{\mu,\sigma} & \text{if} \quad \sum_{i=1}^{n} \varphi_{d_i}^{\mu,\sigma} \approx 1 \\ 0 \end{cases} \tag{27}$$

The weighted attenuation due to each particle size at a given frequency can be calculated using Eq. 28 for all distributions defined by the possible values of "μ" and "σ." The total weighted attenuation due to all particle sizes at a given frequency is given by Eq. 29 and the calculated effective attenuation of the pulse can then be obtained using Eq. 30.

$$C_{d_i,\mathrm{f}} = w_{\mathrm{f}} \frac{3\varphi_{d_i}^{\mu,\sigma}}{4\pi r_i^3} \left(\sum\nolimits_s + \sum\nolimits_a \right) \tag{28}$$

$$\alpha_{w_{\mathrm{f}}}^{C} = \sum_{i=1}^{n} C_{d_i,\mathrm{f}} \tag{29}$$

$$\alpha_{\mathrm{eff}}^{\mathrm{C}} = \sum_{f_{\min}}^{f_{\max}} \alpha_{\mathrm{wf}}^{\mathrm{C}} \tag{30}$$

Similarly, the measured weighted attenuation at each frequency and the measured effective attenuation of the pulse can be obtained using Eqs. 31 and 32.

$$\alpha_{\mathrm{wf}}^{\mathrm{M}} = \alpha_{\mathrm{f}}^{\mathrm{M}} w_{\mathrm{f}}^{\mathrm{M}} \tag{31}$$

$$\alpha_{\mathrm{eff}}^{\mathrm{M}} = \sum_{f_{\min}}^{f_{\max}} \alpha_{\mathrm{wf}}^{\mathrm{M}} \tag{32}$$

The volume fraction of particles in the system can be predicted using the superposition principle (Eq. 33) and the error between known and predicted concentration is given by Eq. 34.

$$\phi^{\mathrm{C}} = \frac{\alpha_{\mathrm{eff}}^{\mathrm{M}}}{\alpha_{\mathrm{eff}}^{\mathrm{C}}} \tag{33}$$

$$\Delta_{\phi} = \left| \phi - \phi^{\mathrm{C}} \right| \tag{34}$$

The following constraints have to be satisfied by the predicted attenuation for the log-normal parameters to define the particle size distribution in the system.

$$\sum_{f_{\min}}^{f_{\max}} \alpha_{\mathrm{wf}}^{\mathrm{C}} \phi^{\mathrm{C}} \approx \sum_{f_{\min}}^{f_{\max}} \alpha_{\mathrm{wf}}^{\mathrm{M}} \quad \text{and,} \quad \Delta_{\phi} \to 0 \tag{35}$$

Hence, the best-fit of the parameters of log-normal distribution can be obtained by minimizing the sum of absolute errors between measured and predicted attenuation and the error in attenuation due to "Δ_{ϕ}" at each frequency.

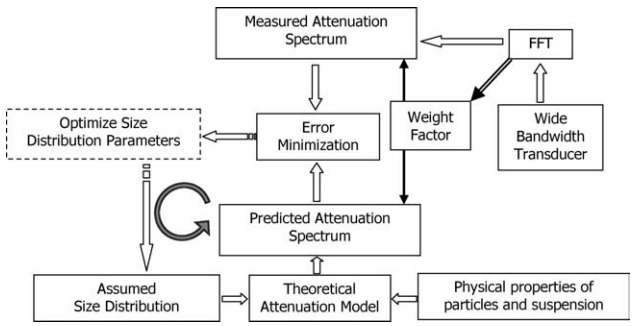

Figure 18. Deconvolution algorithm for PSD determination.

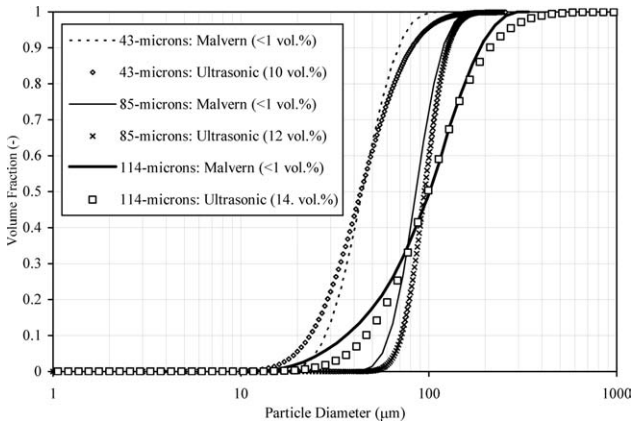

Figure 19. Comparison of measured PSD using ultrasonic technique and Malvern Mastersizer® for 43-, 85-, and 114-μm particles suspension in DI-water.

$$E^{\mu,\sigma} = \sum_{f_{\min}}^{f_{\max}} \left(\left| \alpha_{\mathrm{wf}}^{\mathrm{M}} - \phi^{C} . \alpha_{\mathrm{wf}}^{\mathrm{C}} \right| + \Delta_{\phi} \alpha_{\mathrm{wf}}^{\mathrm{C}} \right)$$
$$\min\{E^{\mu,\sigma}\} \rightarrow \varphi_{d}^{\mu,\sigma} \tag{36}$$

The average size and standard deviation of particles in the system are calculated from the best-fit log-normal parameters "μ" and "σ" using the relationships given in Eq. 37.

$$d_{\mathrm{avg}} = e^{\mu + 0.5\sigma^2}$$
$$\sigma_{\mathrm{Dist}} = \sqrt{(e^{\sigma^2} - 1) e^{2\mu + \sigma^2}} \tag{37}$$

Figure 19 shows the measured PSD using ultrasonic technique for 43, 85, and 114-μm particles at 10, 12, and 14 vol %, respectively. Figure 20 shows the measured PSD using ultrasonic technique for 119, 156, and 202-μm particles at

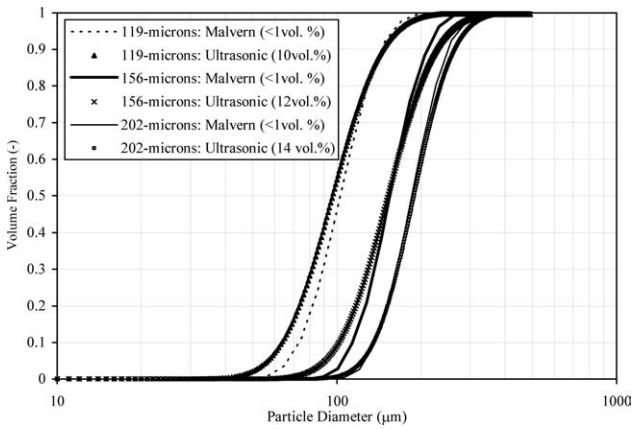

Figure 20. Comparison of measured PSD using ultrasonic technique and Malvern Mastersizer® for 119-, 156-, and 202-μm particles suspension in DI-water.

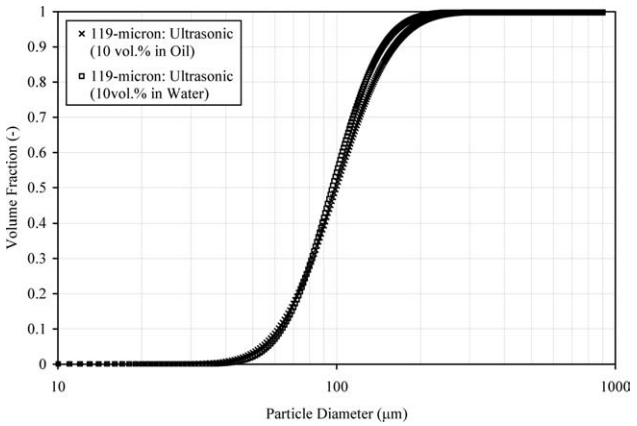

Figure 21. Comparison of measured PSD using ultrasonic technique for 119-μm glass beads suspension (10 vol %) in DI-water and canola oil.

10, 12, and 14 vol %, respectively. Offline PSD measured using Malvern Mastersizer® at concentrations less than 1 vol % are also shown in these figures. Performance of the novel ultrasonic spectroscopy technique was also tested for glass beads suspension in canola oil and aluminum oxide suspension in DI-water. Figure 21 shows that the measured PSDs for 119-μm glass beads (10 vol %) in canola oil is similar to the measurements obtained in the DI-water suspension. Figure 22 shows a comparison of the PSDs measured using ultrasound at 8 and 12 vol % concentration for 112-μm aluminum oxide with the results obtained using Malvern Mastersizer® (<1 vol %). The PSDs measurements were made using 3.4 MHz transducer with the search domain set between "$d_{\min} = 1$ μm" to "$d_{\max} = 1000$ μm" and the attenuations were predicted using the modifications proposed to the Morse and Ingard[17] model. The PSD measurements were obtained from the average of five pulses sampled at each concentration to obtain the mean attenuation spectrum.

Ultrasonic technique uses the volume-weighted absorption and scattering losses as opposed to projected surface area

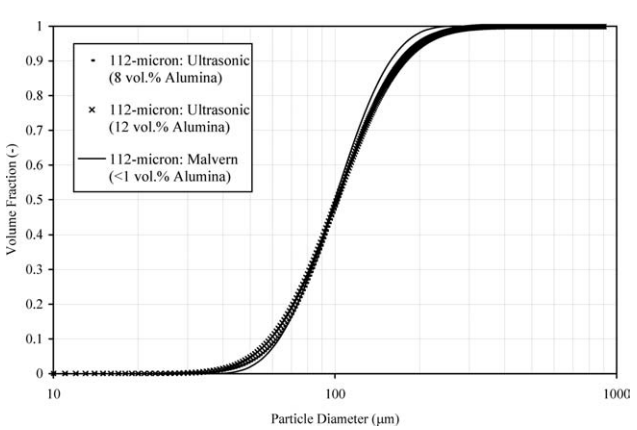

Figure 22. Comparison of measured PSD using ultrasonic technique for 112-μm aluminum oxide suspension (8 and 10 vol %) in DI-water with the measurements of Malvern Mastersizer®.

based laser diffraction measurements (Malvern Mastersizer®) for PSD calculations. Based on the measurement principle different characteristics of the particle are measured and hence some differences between the PSDs generated by different measurement techniques are unavoidable. The measurements obtained using ultrasonic technique is more representative as compared to Malvern Mastersizer® which operates at concentrations less than 1 vol % and can lead to significant sampling errors. Ultrasound has a good penetration depth (~50 mm) even under dense conditions and unlike laser diffraction measurements it can operate in opaque suspensions. Furthermore, the PSD measurements in the current study are based on the average of five pulses sampled at each concentration to obtain the mean attenuation spectrum. Higher data acquisition rate will enable signal averaging and hence generate a more representative spectrum.

Conclusions

Attenuation measurements in dense suspensions of particles were investigated to study the effect of particles concentration and measurement frequency in the intermediate wave propagation regime. Nonlinearity in the measured attenuation with increase in concentration was attributed to the effect of shift in the frequency spectrum. Particle polydispersity effects on the attenuation measurements were studied using particles with the same average size but different distributions. It was observed that higher concentration of larger particles resulted in a decrease in the measured attenuation. The deviations at higher concentrations were attributed to the measurement of low-angle scattered waves by the detector. The inclusion of detector size in the calculation of attenuation using the Morse and Ingard[17] model resulted in good agreement with the measurements. A weighting factor was used to replicate the measurement conditions in the calculated attenuation spectrum. The PSD determined using the improvements proposed in this study showed that a model based technique can be used for measurements in the intermediate wave regime at high suspension concentrations. The measured PSDs showed good agreement with the results of off-line Malvern Mastersizer®. Further improvements in the ultrasonic based measurements can be obtained using higher sampling rates and wider pulse bandwidth.

Notation

A_{i-1} = initial amplitude (v)
A_i = final amplitude (v)
c = acoustic velocity (m s^{-1})
$C_{d,f}$ = calculated weighted attenuation (Np m^{-1})
d = particle diameter (μm)
$E^{\mu,\sigma}$ = total error in predicted attenuation
f = frequency (MHz)
h_m = Hankel function
j_m = Bessel function
kr = nondimensional wavenumber (-)
m = integer (-)
N = number of particles (-)
P_{i-1} = initial power
P_i = final power
$\dot{P}_m$ = Legendre function
r = particle radius (m)
w_f = weighting factor for attenuation at constituent frequency (-)
x = path length of radiation in slurry (m)

Greek letters

α = attenuation (Np m^{-1})
α_M = measured attenuation (Np m^{-1})
α_{wf}^C = calculated weighted attenuation at each frequency (Np m^{-1})
α_{eff}^C = calculated effective attenuation of pulse (Np m^{-1})
α_{wf}^M = measured weighted attenuation at each frequency (Np m^{-1})
α_{eff}^M = measured effective attenuation of pulse (Np m^{-1})
$\alpha_{T,PD}$ = total attenuation for polydispersed particles (Np m^{-1})
$\alpha_{T,MD}$ = total attenuation for mono-dispersed particles (Np m^{-1})
α_i = attenuation due to ith size fraction (Np m^{-1})
α_{sc} = scattering attenuation (Np m^{-1})
α_t = thermal attenuation (Np m^{-1})
α_v = viscous attenuation (Np m^{-1})
β_m = surface admittance (-)
Δ = measurement angle
Δ_ϕ = error between known and calculated volume fraction (-)
δ_v = viscous layer thickness (m)
ϕ = particle volume fraction in suspension (-)
ϕ^C = calculated total volume fraction
$\varphi_d^{\mu\sigma}$ = calculated volume fraction in log-normal distribution
κ = compressibility (m^2 N^{-1})
λ = wavelength (m^{-1})
μ = geometric mean size (μm)
μ_f = fluid viscosity (N s m^{-2})
σ = geometric standard deviation
σ_{Dist} = standard deviation of distribution
ω = angular frequency (rad s^{-1})
ϑ = scattering angle
ρ_p = particles density (kg m^{-3})
ρ_f = fluid density (kg m^{-3})
$\sum_a$ = absorption c/s area (m^2)
$\sum_s$ = scattering c/s area (m^2)

Subscripts

f = frequency (MHz)
i = particle size index ($i = 1 \ldots n$) or concentration index ($i = 1 \ldots m$)

Literature Cited

1. Pellam JR, Galt JK. Ultrasonic propagation in liquids. I. Application of pulse technique to velocity and absorption measurements at 15 megacycles. *J Chem Phys*. 1946;14:608–613.
2. Pinkerton JMM. A pulse method for measuring ultrasonic absorption in liquids. *Nature*. 1947;160:128–129.
3. Andrea J, Joyce P. 30 to 230 megacycle pulse technique for ultrasonic absorption measurements in liquids. *Br J Appl Phys*. 1962;13:462–467.
4. Holmes AK, Challis RE, Wedlock DJ. A wide bandwidth study of ultrasound velocity and attenuation in suspensions: comparison of theory and experimental measurements. *J Colloid Interface Sci*. 1993;156:261–268.
5. Riebel U. Methods of and an apparatus for ultrasonic measuring of the solids concentration and particle size distribution. US Patent 4,706,509, 1987.
6. McClements DJ. Ultrasonic characterization of emulsions and suspensions. *Adv Colloid Interface Sci*. 1991;37:33–72.
7. Dukhin AS, Goetz PJ. *Ultrasound for characterizing colloids—particle sizing, zeta potential, rheology*. In: Dukhin AS, Goetz PJ, editors. *Studies in Interface Science*, Vol.15. Boston: Elsevier, 2002.
8. Epstein PS, Carhart RR. The absorption of sound in suspensions and emulsions. I. Water fog in air. *J Acoust Soc Am*. 1941;25:553–565.
9. Allegra JR, Hawley SA. Attenuation of sound in suspensions and emulsions. *J Acoust Soc Am*. 1972;51:1545–1564.
10. McClements JD, Hemar Y, Herrmann N. Incorporation of thermal overlap effects into multiple scattering theory. *J Acoust Soc Am*. 1999;105:915–918.

11. Waterman PS, Truell R. Multiple scattering of waves. *J Math Phys*. 1961;2:512–537.
12. Lloyd P, Berry MV. Wave propagation through an assembly of spheres. *Proc Phys Soc*. 1967;91:678–688.
13. Harker AH, Temple JAG. Velocity and attenuation of ultrasound in suspensions of particles in fluids. *J Phys D: Appl Phys*. 1988;21: 1576–1588.
14. Gibson RL, Toksoz MN. Viscous attenuation of acoustic waves in suspensions. *J Acoust Soc Am*. 1989;85:1925–1934.
15. Temkin S. Viscous attenuation of sound in dilute suspensions of rigid particles. *J Acoust Soc Am*. 1996;100:825–831.
16. Bohren C, Huffman D. *Absorption and Scattering of Light by Small Particles*. New York: John Wiley & Sons, 1983.
17. Morse PM, Ingard KU. *Theoretical Acoustics*. New York: McGraw Hill, 1968.
18. Zwietering TN. Suspension of solid particles in liquid by agitators. *Chem Eng Sci*. 1958;8:244–253.
19. Stolojanu V, Prakash A. Characterization of slurry systems by ultrasonic techniques. *Chem Eng J*. 2001;84:215–222.
20. Atkinson CM, Kyotomaa HK. Acoustic wave speed and attenuation in suspensions. *Int J Multiphase Flow*. 1992;18:577–592.
21. Spelt PDM, Norato MA, Sangani AS, Tavlarides LL. Determination of particle size distributions from acoustic wave propagation measurements. *Phys Fluids*. 1999;11:1065–1080.
22. Shukla A. Size and concentration measurement in slurries by ultrasonic methods. M.E.Sc. Thesis. University of Western Ontario, London, 2003.
23. Shukla A. Ultrasonic techniques for dispersed phase characterization. PhD Thesis. University of Western Ontario, London, Ontario, 2007.
24. Prakash A, Shukla A, Rohani S. Method and apparatus for ultrasound monitoring of particle size distribution. U.S. Pat. Appl. 61177029, 2009.

Manuscript received May 27, 2009, revision received Oct. 13, 2009, and final revision received Jan. 14, 2010.